Atmospheric pressure atomic layer deposition for tight ceramic nanofiltration membranes: Synthesis and application in water purification

Shang, Ran; Goulas, A; Tang, CY; de Frias Serra, Xavier; Rietveld, Luuk; Heijman, Bas

DOI
10.1016/j.memsci.2017.01.023

Publication date
2017

Document Version
Accepted author manuscript

Published in
Journal of Membrane Science

DOI: http://dx.doi.org/10.1016/j.memsci.2017.01.023

To appear in: *Journal of Membrane Science*

Received date: 12 November 2016

Revised date: 1 January 2017

Accepted date: 13 January 2017

Cite this article as: Ran Shang, Aristeidis Goulas, Chuyang Y. Tang, Xavier de Frias Serra, Luuk C. Rietveld and Sebastiaan G.J. Heijman, Atmospheric pressure atomic layer deposition for tight ceramic nanofiltration membranes: synthesis and application in water purification, *Journal of Membrane Science,* http://dx.doi.org/10.1016/j.memsci.2017.01.023

Atmospheric pressure atomic layer deposition for tight ceramic nanofiltration membranes: synthesis and application in water purification

Ran Shang [a, d], Aristeidis Goulas [b], Chuyang Y. Tang [c], Xavier de Frias Serra [a, e], Luuk C. Rietveld [a], Sebastiaan G.J. Heijman [a]

[a] *Department of Sanitary Engineering, Faculty of Civil Engineering and Geosciences, Delft University of Technology, P.O. Box 5048, 2600 GA Delft, The Netherlands*

[b] *Delft IMP B.V., 2629 JD Delft, The Netherlands*

[c] *Department of Civil Engineering, The University of Hong Kong, Pokfulam HW619B, Hong Kong*

[d] *School of Environmental Science and Engineering, Huazhong University of Science and Technology, Wuhan 430074, China*

[e] *IQS School of Engineering, Universitat Ramon Llull, Via Augusta 390, 08017 Barcelona, Spain*

Abstract:

Tight ceramic nanofiltration (NF) membranes allow efficient separation of organic matter and ions for advanced water treatment. These membranes are typically produced by the sol-gel method. Recently, atomic layer deposition (ALD), a self-limiting gas phase coating technique, has been explored for membrane fabrication and modification. In this work, the synthesis of tight ceramic NF membranes is demonstrated using atmospheric pressure ALD (APALD), which is operated without a vacuum-generation system compared to the commonly reported vacuum-based ALD method. Titanium dioxide was coated on nano-porous membrane substrates using merely one to three cycles of APALD. The average size of active pores was effectively narrowed by 0.2 nm, from 0.7 nm to 0.5 nm. In addition, the size distribution of the active pores became more uniform after the APALD modification. The fabricated tight ceramic NF membranes had a molecular weight cut-off (MWCO) ranging from 260 to 380 Da while maintaining high water permeability at 11-16 L m^{-2} h^{-1} bar^{-1}, which is notably higher than the commercial tight polymeric NF and sol-gel-made tight ceramic NF membranes. It was observed that conformal TiO_2 thin films can be deposited on planar surfaces under the APALD with a growth rate of 0.39 nm per cycle, while the deposition in the membrane micropores was at a lower rate, estimated as 0.05 nm per cycle.

Keywords:

Ceramic membrane filtration; nanofiltration; atmospheric pressure atomic layer deposition; water treatment

Abbreviations

AFM	atomic force microscopy
ALD	atomic layer deposition
APALD	atmospheric pressure atomic layer deposition
BET	Brunauer-Emmet-Teller theory
GPC	growth-per-cycle
HPLC	high performance liquid chromatography
MF	microfiltration
MW	molecular weight
MWCO	molecular weight cut-off
NF	nanofiltration
PEG	polyethylene glycols
RO	reverse osmosis
SEC	size exclusion chromatography
SEM	scanning electron microscope
TMP	trans-membrane pressure
UF	ultrafiltration

Nomenclature

$C_{i,feed}$	PEG concentration in the membrane's feed solution (-)
$C_{i,permeate}$	PEG concentration in the membrane's permeate solution (-)
d_s	molecular size of PEG tracers (nm)
J	membrane flux (L m^{-2} h^{-1})
$L_{p,20℃}$	membrane's water permeability at 20 °C (L m^{-2} h^{-1} bar^{-1})
ΔP	transmembrane pressure (bar)
R_q	root mean square roughness (nm)
R_a	roughness average (nm)
R_i	rejection rate of PEG (-)
S_{MW}	standard deviation of the molecular weight distribution (-)

T	temperature of water (°C)

Greek letters

$\sigma(MW_s)$	reflection coefficient for a PEG with a molecular weight of MW_s (-)
η_{20} and η_T	permeate viscosity at 20 °C and at the measured water temperature (Pa·s)

1. Introduction

Since the development of synthetic membranes in the 1960s, the application of membrane filtration in water treatment has grown exponentially in recent decades [1-4]. Membrane technology, including ultrafiltration (UF), microfiltration (MF), nanofiltration (NF) and reverse osmosis (RO), has been widely deployed in drinking water purification and wastewater treatment. In recent years, inorganic/ceramic UF and MF membranes have gained increased attention. Although their price is higher, ceramic membranes have many advantages over traditional polymeric membranes, including high mechanical strength, high chemical and thermal resistance, long lifespans, and recyclability as raw ceramic material [5, 6].

An increasing number of recent studies have also focused on (hydrophilic) ceramic NF membranes [5, 7-15]. The ceramic NF has been successfully used to treat various waste streams in full-scale, including, among others, dye removal from textile wastewater and treatment of oily wastewater [13, 16]. In our previous work, a commercial loose ceramic NF membrane (450 Da, Inopor GmbH, Germany) was applied to directly filter domestic wastewater for water reclamation and resource recovery [17, 18]. The tested membranes showed excellent anti-fouling properties, but the rejection of dissolved organic matter and ionic compounds was not satisfactory: it was lower than that of the polymeric (tighter) NF

membranes [17]. Therefore, a scalable tight ceramic NF membrane is expected to facilitate a number of innovative applications for water reuse and wastewater treatment. Despite several lab-scale studies on tight ceramic NF membranes (molecular weight cut-off (MWCO) < 400 Da) [8-10, 12, 15, 19], a majority of the commercially available ceramic NF membranes belong to the category of loose NF membranes (> 400 Da MWCO), with the tightest reaching 450 Da MWCO [7].

It remains a challenge to develop tight ceramic NF membranes [20], partly because they are commonly made via the sol-gel method. The process involves conversion of monomers into a colloidal solution (sol) that acts as the precursor for an integrated network (gel) of either discrete particles (so-called particulate sol-gel route [9]) or network polymers (so-called polymeric sol-gel route [12]). A major limitation of the particulate sol-gel method is the resulting low permeability of the membranes: e.g. 0.5 - 1.5 L m^{-2} h^{-1} bar^{-1} for 200 Da ceramic NF membranes [8, 9, 15, 19]. The low water permeability is a result of the thick coating layers (up to 1 µm of dip-coated layers [15]). Using the polymeric sol-gel method, smaller particles can be formed in the polymeric sol and thinner separation layers can be coated. The result is improved water permeability to 2 - 4 L m^{-2} h^{-1} bar^{-1} [10, 12], which is still lower than the permeability of polymeric NF membranes.

The application of atomic layer deposition (ALD), a self-limiting gas phase coating technique for growing atomic-scale thin films [21], has emerged as a potential route for fabrication and modification of ceramic membranes [6, 22, 23]. ALD provides highly uniform and conforming coating of metal oxides on 3-D structures due to alternating, self-limiting saturated surface reactions. The coated layers can be deposited on the pore walls, resulting in the desired pore size reduction. Li, et al. [22] firstly demonstrated the idea of using ALD to reduce the pore

aperture of a water permeation ceramic membrane, who succeeded in narrowing the pore size of an ultrafiltration membrane from 50 nm to about 6.8 nm after deposition of alumina (Al_2O_3). The water permeability of the coated membrane progressively decreased from 1698 L m^{-2} h^{-1} bar^{-1} to 118 L m^{-2} h^{-1} bar^{-1}. A recent study revealed that TiO_2 loose NF membranes can be obtained via ALD using asymmetric substrates of 20 nm pores [23]. The coated membranes showed a pore size of approximately 1 nm. Interestingly, the ALD-modified NF membrane showed excellent water permeability, as high as 48 L m^{-2} h^{-1} bar^{-1}, which is about twice as high as that of the sol-gel-made NF, as reported by Puhlfürß, et al. [7].

Atmospheric pressure atomic layer deposition (APALD) does not involve the use of expensive vacuum-compatible equipment [21] as used in the aforementioned studies. This enables an easier scale-up approach towards large-volume manufacturing. Although APALD has already been demonstrated for coating (nano-)particles [24-26] and nonporous planar surfaces [27], this technique has not yet been applied to deposit thin films on porous ceramic membranes.

In this study, we applied APALD to fabricate tight ceramic NF membranes with high water permeability. The effect of APALD on the water permeability, rejection of polyethylene glycols (PEGs) and the MWCO of the coated membranes was investigated. The influence of APALD coating on pore size distribution is elucidated based on the Brunauer-Emmet-Teller (BET) theory as well as a pore model based on the polyethylene glycols' rejection profile.

2. Materials and Methods

2.1 Substrate membranes

Commercial ceramic NF membranes (Inopor GmbH, Germany) were used as the substrate for APALD coating. The Inopor membrane has a single-channel tubular configuration with an inner diameter of 7 mm, an outer diameter of 10 mm, a length of 100 mm) , and an effective filtration area of 0.00163 m^2. The geometry of the membrane and calculation of the effective filtration area are described in the Supplementary Material (Figure S1 and Equation S1). The cross-section structure of the pristine membrane (Figure 1) was analysed using a scanning electron microscope (SEM, FEI Nova NanoSEM 450, USA). The separation layer of the received membrane, which is located at the inner surface of the tubular membrane, is made of titanium dioxide (TiO_2) with a porosity of 30%, as described by the manufacturer, and the other layers are made of alumina (Al_2O_3). These membranes have an MWCO of 450 Da as claimed by the supplier. However, great variation in actual MWCO of these membranes were observed, and 6 membranes with MWCO being close to 450 Da were pre-selected for the APALD coating.

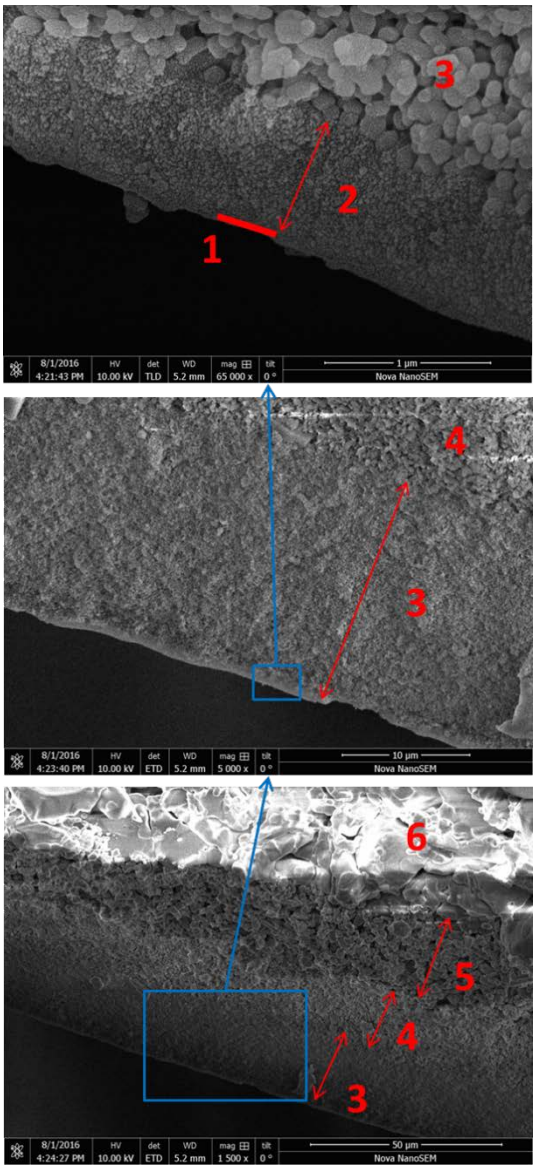

Figure 1. Scanning electron microscope (SEM) micrographs of cross-section of the as-received pristine membrane. 1: separation layer (0.05 µm); 2-5: intermediate layers (0.8 µm; 18 µm; 15 µm; 18 µm); 6: support layer.

2.2 Atmospheric pressure atomic layer deposition (APALD)

A flow-type APALD reactor (Delft IMP B.V., Delft, the Netherlands) was used for coating TiO_2 onto the substrates, including the inner and outer surface of the channel (Figure 2). Titanium

tetrachloride, $TiCl_4$ (Sigma-Aldrich/Fluka, the Netherlands) and demineralized water vapour, H_2O, both diluted in a stream of nitrogen gas, N_2 (HiQ 5.0, Linde Gas Benelux, the Netherlands), were used as precursors. In the reactor, the precursors flowed over the substrate in a direction parallel to its surface. When $TiCl_4$ was exposed to the substrate, it chemisorbed and the following reaction (A) took place:

$$n(-OH)^* + TiCl_4(g) \rightarrow (-O-)_n TiCl_{4-n}{}^* + nHCl(g) \quad \text{A}$$

where the asterisks denote the surface species.

Thereafter, the excessive $TiCl_4$ and generated hydrochloric acid, *HCl*, vapours were purged using dry N_2, and then the co-reactant H_2O was introduced to finish one cycle of coating with the following reaction (B):

$$(-O-)_n TiCl_{4-n}{}^* + (4-n)H_2O(g) \rightarrow (-O-)_n Ti(OH)_{4-n}{}^* + (4-n)HCl(g) \quad \text{B}$$

Thereafter, the reactor was purged again to cleanse the residual H_2O and produced *HCl* vapours. The alternating A-B cycles led to a progressively increasing thickness of TiO_2 on the substrates. In the current study, the APALD reactor was heated to 180 ^{o}C during the process by using an infrared lamp connected to a digital temperature probe. The precursor exposure and purging times were 5 s and 300 s, respectively. The conditions are summarized in Table S1 of the Supplementary Material. A long purging time of 300 s was used in this study to prevent uncontrolled growth of TiO_2 inside the pores because the excessive precursors need to diffuse to the nitrogen purging gas and the diffusion process will take longer than the time needed to purge a non-porous surface [28].

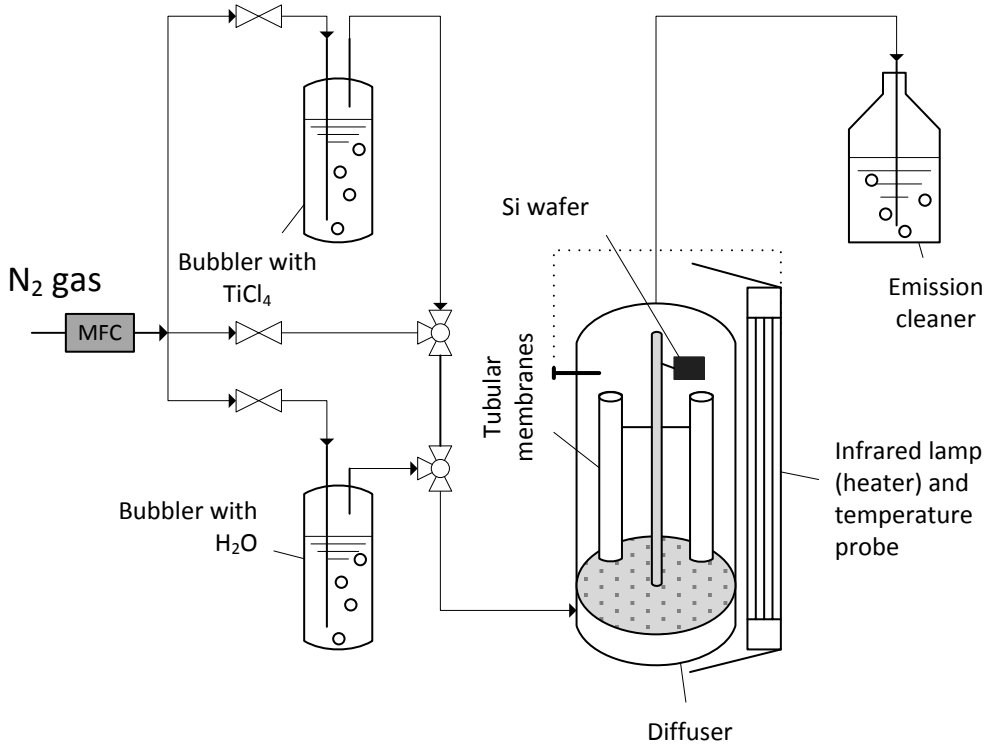

Figure 2. Schematic overview of the APALD setup

The substrate membranes were fixed vertically in the up-flow reactor (Figure 2). Silicon witness wafers were placed next to the membranes to monitor the thickness of the coated layer which was measured by an ellipsometer (M-2000F, J.A.Woollam Co. Inc., USA). By analysing the change of light polarization, the ellipsometer determines the thickness of thin layers within a few angstroms of accuracy. However, the substrate membranes used in this study have a tubular configuration. Direct measurement of coating thickness on the curved surface of the separation layer was therefore not feasible. Instead, surrogate silicon wafers of 1 cm x 2 cm with a flat surface were used for monitoring the layer growth by the ellipsometer.

198 The thickness of the native oxide layer (SiO_2) on the surface of each silicon wafer was
199 measured as a reference using the ellipsometer. After the coating of the wafers, the
200 thickness of the coated TiO_2 layer was again determined using the ellipsometer, deducting
201 the thickness of the premeasured SiO_2 layer.

202 Additionally, the silicon wafers were used to measure the growth-per-cycle (GPC) in the
203 APALD system. The silicon wafers were coated with TiO_2 via 1, 3, 8 and 13 cycles of APALD,
204 using the same coating conditions as used for membrane coating. The obtained linear
205 regression between coating thickness and the coating cycles describes the process GPC.

206 The topography and surface roughness of the silicon wafers were also analysed in order to
207 check the coating quality, using an atomic force microscopy (AFM, Dimension Fast scan
208 Bruker). Again, the analysis was only done on the silicon wafers. The AFM measurements of
209 the pristine and coated silicon wafers were performed ex-situ, right after the deposition. The
210 surface roughness was quantitatively identified by both the root mean square roughness
211 (R_q) and the roughness average (R_a).

212

213 2.3 Membrane characterization and performance

214 2.3.1 Molecular weight cut-off (MWCO)

215 The MWCO is defined as the molecular weight of a tracer molecule that is retained with 90%
216 efficiency by the membrane. Polyethylene glycols (PEGs) of molecular weights ranging from
217 200 Da to 1000 Da were used as the tracer molecules. The PEG molecules are non-charged,
218 and therefore their rejection by membranes is the result of steric rejection. A feed solution,
219 containing a mixture of the PEGs with a concentration of 0.6 g L^{-1} of each, was filtered

through the pristine and coated membranes, at room temperature and in cross-flow mode. The feed solution permeated the wall of the tubular ceramic membranes (inside-out) under a constant trans-membrane pressure (TMP) of 4 bar and a cross-flow velocity greater than 1 m s^{-1}. The PEG molecules that are smaller than the diameter of the pores in the membrane pass through it; the larger molecules are retained by the membrane and return to the feed solution. Use of mixture of PEGs tends to underestimate the MWCO and pore size of the membrane as the larger solutes will hinder the permeation of smaller ones. The influence of TMP and PEG concentration on the MWCO measurement was evaluated. The results showed that an increased TMP led to a decreased MWCO, while the concentration of PEG, from 0.2 to 2 g L^{-1} for each compound, showed no influence on the measured MWCO (Figure S2 and S3 in the Supplementary Material). In this study, a TMP of 4 bar was selected in order to compare the results with that measured by the manufacturer [7].

To calculate the MWCO, both the feed solution and the permeate solution were analysed by a high-performance liquid chromatography system (HPLC, Shimadzu, Japan) equipped with size exclusion chromatography columns (SEC, 5 µm 30 Å, PSS Polymer Standards Service GmbH, Germany). These analyses generated molecular weight distribution curves of the dissolved PEG molecules in the feed and permeate solutions. The corresponding retention curves were then plotted by determining the rejection rate of a PEG with certain molecular weight (R_i) using the following equation:

$$R_i(\%) = \left(\frac{C_{i,feed} - C_{i,permeate}}{C_{i,feed}}\right) \qquad (1)$$

where, $C_{i,feed}$ and $C_{i,permeate}$ are the PEG concentration in the feed and permeate solutions. Afterwards, the experimental rejection curves were described by a log-normal model as a function of *MW* and *MWCO*, given by Eq. 2 [29, 30]:

$$\sigma(MW_s) = \int_0^{MW_s} \frac{1}{S_{MW}\sqrt{2\pi}} \frac{1}{MW} \exp\left[-\frac{(\ln(MW)-\ln(MWCO)+0.56S_{MW})^2}{2S_{MW}^2}\right] dMW \quad (2)$$

where $\sigma(MW_s)$ is the reflection coefficient for a PEG with a molecular weight MW_s, S_{MW} is the standard deviation of the molecular weight distribution.

Further, it is assumed that the pore size of the NF membrane follows a log-normal distribution, and the separation mechanism is based on size exclusion with negligible solute diffusion. The molecular size of PEG tracers (d_s in nm) is correlated to their molecular weight (*MW* in Da) [30]:

$$d_s = 0.065(MW)^{0.438} \quad (3)$$

2.3.2 Permeability of the membranes

Water filtration performance was examined by the temperature-corrected permeability. Demineralized water was filtered at a constant TMP of 4 bar. Membrane fluxes and water temperature were monitored. An increase of water temperature, from 17 to 25 °C, was observed during the water filtration experiments due to heat conduction from the cross-flow pump. The temperature-corrected permeability at 20 °C was calculated using the following equation:

$$L_{p,20℃} = \frac{J}{\Delta P} \cdot \frac{\eta_T}{\eta_{20}} = \frac{J \cdot e^{-0.0239 \cdot (T-20)}}{\Delta P} \quad (4)$$

where $L_{p,20℃}$ is the permeability at 20 °C (L m^{-2} h^{-1} bar^{-1}), J is the measured membrane flux (L m^{-2} h^{-1}), *ΔP* is the measured TMP (bar), *T* is temperature of water (°C), and η_{20} and η_T are the permeate viscosity at 20 °C and at the measured water temperature.

2.3.3 Active pore size and BET pore size determination

The active pores, which determine the steric rejection of the membrane, are defined as the pores with full coverage over the membrane surface [31]. The active pore size distribution was derived from the PEG rejection profile using the log-normal model as described in section 2.3.1.

Physical adsorption of gas molecules on a surface as described by the Brunouer-Emmet-Teller (BET) theory offers another tool to measure pore size distribution in the ceramic membranes. However, the BET method detects pores of various pore sizes, including more than the active pores [32]. Therefore, the pore size distribution of the pristine membranes and the coated membranes were also characterized using the CO_2 adsorption method according to the BET theory. The adsorption/desorption isotherms with CO_2 as adsorbate were recorded at 298 K using a pore size analyser (Autosorb 6B, Quantachrome Instruments, USA). Prior to the adsorption measurements, the tubular membranes were crushed using a mortar and pestle, and degassed in a vacuum for 16 h at 120 °C. The dry samples weight obtained after the pre-treatment was taken into account in the calculations.

In BET measurements, the physical adsorption of nitrogen (N_2) gas molecules at a temperature of 77 K is typically used instead of CO_2 adsorption. However, the drawback of using N_2 as an adsorbate for measuring micropores is the very slow diffusion rate into the micropores at a relatively low temperature (77 K) [33]. Therefore, CO_2 adsorption at 298 K was preferred due to the faster kinetics under the higher operational temperature. Another advantage of using CO_2 as an adsorbate is that the pore volume can be accurately differentiated in the pore size range between 0.3 to 1.5 nm.

3. Results and discussions

287 3.1 Thickness and growth kinetics of TiO_2 layers on silicon wafers by APALD

288 The estimated thickness of deposited TiO_2 films on the silicon wafers grows linearly with the
289 increment of coating cycles by the APALD (Figure 3). The GPC is determined to be 0.39 nm
290 per cycle, as obtained from the slope of the linear regression. A growth rate of a few
291 angstrom is typical for ALD under atmospheric pressure on a planar surface, for instance on
292 the surface of particles [25, 34]. In comparison, for ALD of TiO_2 under vacuum conditions, a
293 lower GPC of 0.04-0.06 nm is reported [35-39], because vacuum prevents the formation of
294 precursor and co-reactant multilayers on the substrate surface [25]. In addition, it is more
295 difficult to purge the excess precursors and reaction by-products under atmospheric
296 pressure, albeit the adoption of longer purging times.

297 Despite the relatively high GPC, conforming TiO_2 layers were deposited using the APALD
298 technique, as evidenced by the AFM analysis of the silicon wafers (Figure S4 in the
299 Supplementary Material). The surface roughness of the pristine and coated silicon wafers
300 was between 0.16 and 0.21 nm in terms of root mean square roughness, respectively, and
301 was 0.13 - 0.17 nm in terms of mean roughness. The variation in the measured surface
302 roughness was negligible (always less than 0.05 nm).

303

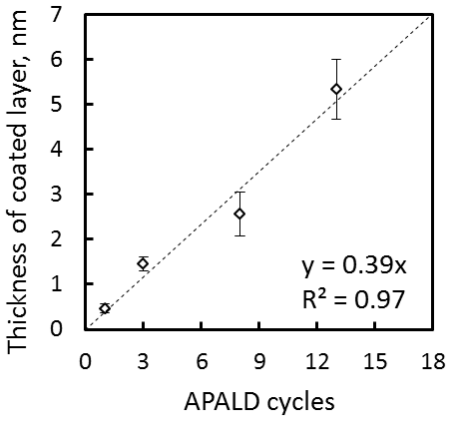

304

Figure 3. Correlation between the thickness of coated TiO_2 layer and the number of APALD cycles for deposition onto silicon wafers. Error bars indicate a standard deviation of 5 measurements.

3.2 Effect of APALD coating on the membrane active pore size and MWCO

The coated membranes showed a considerably higher rejection of PEGs of MW 200-400 Da. Based on the PEG rejection and the log-normal model, the size distributions of the active pores in the pristine membranes and the coated membranes of samples 1, 3 and 5 are depicted in Figure 5. The results of the duplicates, sample numbers 2, 4 and 6, can be found in Figure S5 of the Supplementary Material. The average size of the active pores of the coated membranes narrowed from 0.7 nm to 0.5 nm, after one to three cycles of APALD. Furthermore, the coated membranes have more homogeneously-sized active pores, evidenced by their narrower pore size distribution (Figure 5 b, d and f) and their steeper PEG rejection curves (Figure 5 a, c and e).

Using the CO_2 adsorption method, the pore size distribution in the separation layer of the pristine membranes can be determined. This is because that, in the pristine membranes, only the pores in separation layer fall into the detection range of the applied CO_2 adsorption method (0.3-1.5 nm), since the intermediate layer just underneath the separation layer has a pore size of 5 nm [7]. The majority of pores (90%) were found to be ranging from 0.5 nm to 0.8 nm in the separation layer of the pristine membranes (Figure 6). The measured micropore size distribution in the pristine membranes was consistent with the active pore size distribution derived from the PEG/HPLC-measurements (Figure 5). The pores are expected to be symmetrical over the separation layer, since the separation layer is made

after a single dip-coating of the polymeric sol [7]. In the APALD-coated membranes, the pore size also ranged from 0.5 nm to 0.8 nm, thus showing a similar result as the pristine membranes. When compared to the pristine membranes, the volume of 0.5-0.6 nm pores slightly increased in the coated membranes, while the volume of 0.6-1.4 nm pores was reduced.

The pore size analysis suggested that the growth rate of TiO_2 in micropores was lower than the growth rate on the planar surface of silicon wafer. The metal-source precursor $TiCl_4$ molecule of 0.64 nm [40] tended to preferentially chemisorb in the relatively large pores of 0.7-0.8 nm in the separation layer. Since the size of the precursor is comparable to the size of the pores [41], a maximum of one molecule of $TiCl_4$ was allowed to enter the pore and to chemisorb on the active sites on the pore wall. Therefore, the deposition on the pore wall was likely to be at a much lower rate than the measured growth rate on the planar surface of silicon wafers (0.39 nm per cycle). After one cycle of A-B reaction, the reduction of pore aperture should equal the size of a TiO_2 molecule, reported as 0.04-0.06 nm [35-39]. The MWCO of the coated membranes decreased to 265 – 308 Da after 1, 2 and 3 cycles of APALD, except for sample No. 3 (380 Da) which is likely due to the high MWCO of the No.3 pristine membrane (Figure 7). Results obtained using both MWCO and BET measurements confirmed that there was a clear trend of pore size reduction after the deposition. Based on the BET measurements (Figure 6), we observed that micropores in the pristine membrane ranging from 0.8 to 1.4 nm, counting for about 10% of the total pore volume in the separation layer, disappeared after the APALD. It is a clear evidence that the deposition did take place in the pores. However, it remains a question that which fraction of the deposition (deposition in the pores or deposition on the membrane surface) has predominantly contributed to the observed pore size reduction.

Unlike the previously reported results of macroporous membrane coating using vacuum ALD systems [22, 42, 43], a progressive decrease in MWCO with the increase of the APALD cycles was not observed (Figure 7): the coated NF membranes showed similar MWCO. This observation might be attributed to the pore-size restricted diffusion of the precursors. As the molecular diameter of the reactants (0.64 nm) approaches the pore diameter, the pores may restrict the diffusion of reactants into the membrane pores [41]. As a result, the pore apertures may reach a minimum value, and the pore aperture will not significantly decrease with increased APALD cycles.

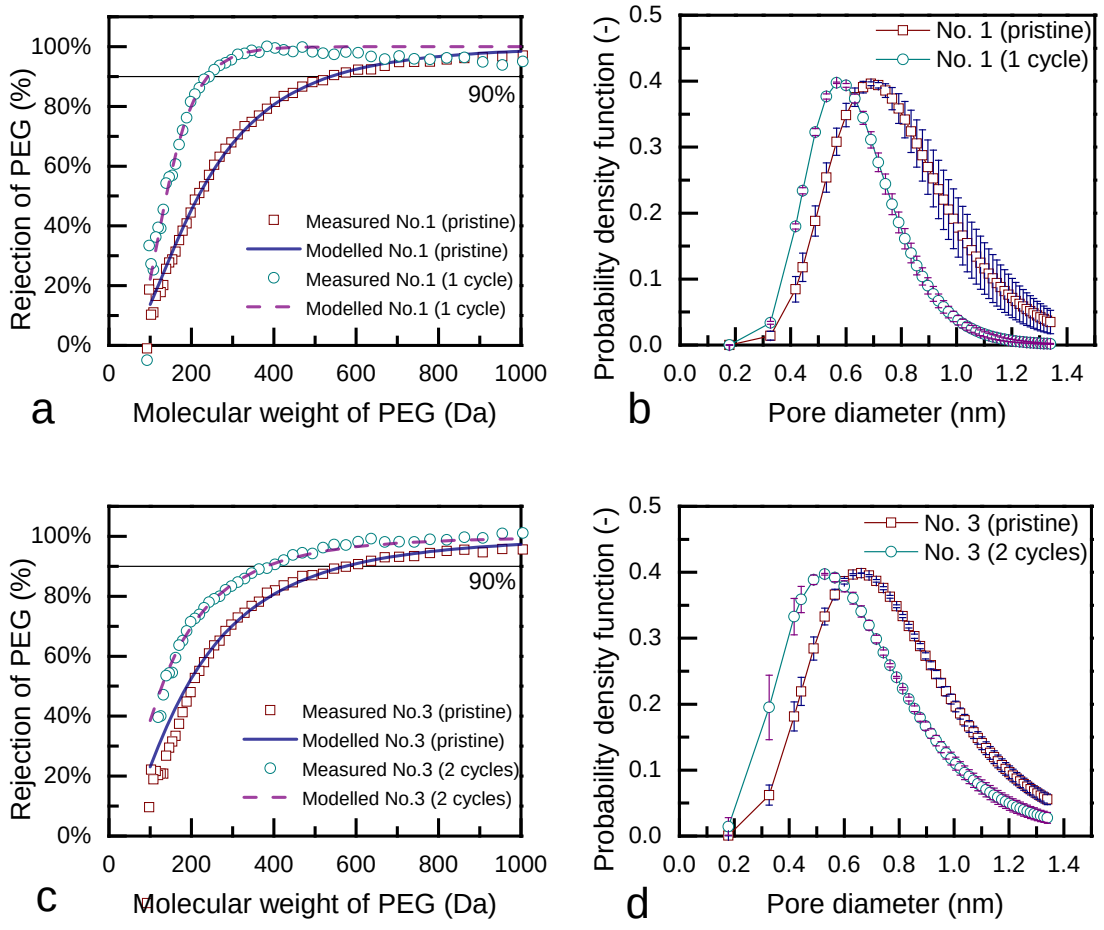

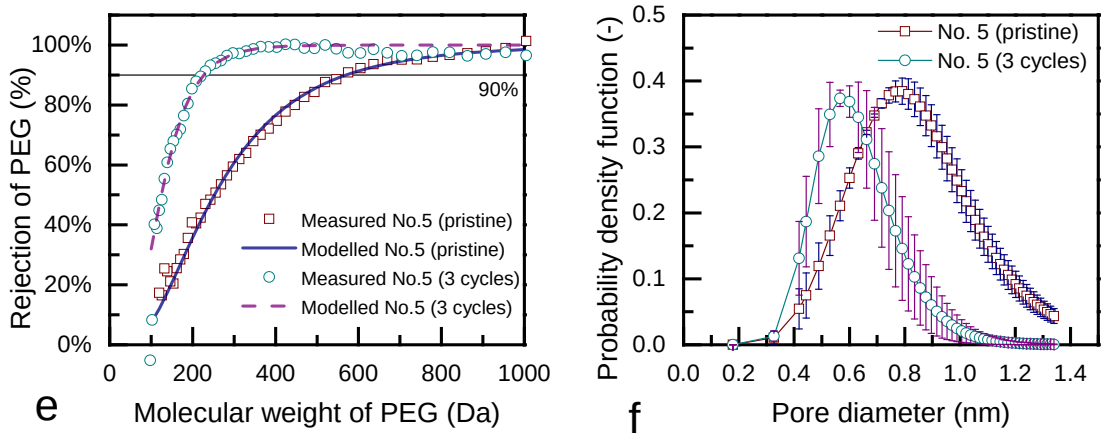

363

364 Figure 5. PEG rejection (a, c and e) and modelled active pore size distribution (b, d and f) of

365 the pristine (substrate) membranes and the coated membranes by APALD (samples No.1,

366 No.3 and No.5). The error bars indicate standard deviation of triplicate samples.

367

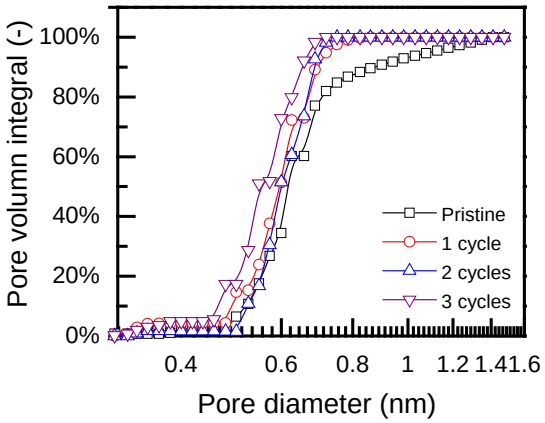

368

369 Figure 6. Size distribution of micropores in the pristine and coated membranes (with number

370 of APALD cycles indicated) measured by CO_2 adsorption.

371

372 In addition, the pore aperture may also be reduced by the growth of TiO_2 on top of the

373 membrane surface at the opening of the pores. The growth on the membrane surface is

374 apparently not influencing the pore sizes. As seen in section 3.1, the growth rate of TiO_2

layers on the membrane surface is approximate 0.39 nm per cycle of APALD. This coated layer build-up on the surface near or at the pore openings may contribute to the reduction of pore size during the first cycle of ALD. Also, the formed TiO_2 layer was expected to be porous, having a larger pore size than the size of the active pores. A study by Nikkola, et al. [44] suggests that the ALD-deposited Al_2O_3 exhibits a loose and porous structure when the number of applied coating cycles is below 50 (nominal coating thickness of 5 nm), and the pore size in this structure is larger than the micropores of the coated polymeric RO membranes.

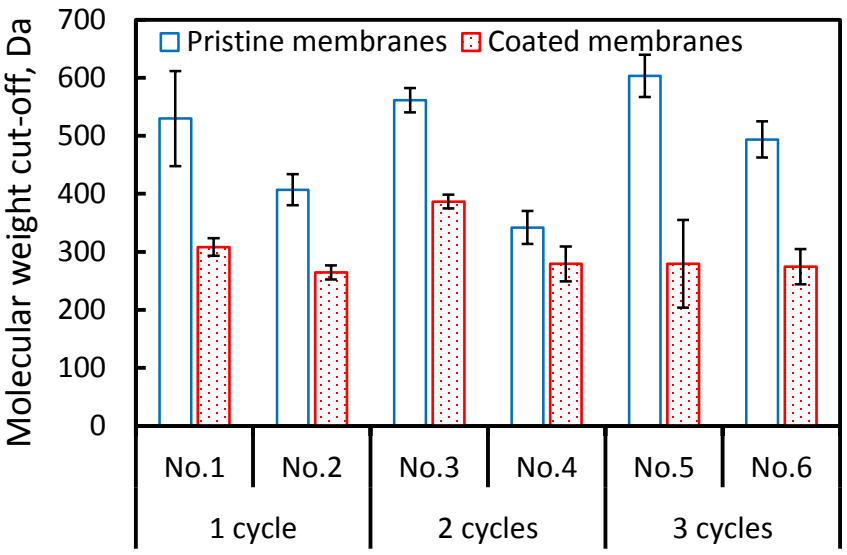

Figure 7. Molecular weight cut-off (MWCO) of the pristine (substrate) membranes and the coated membranes using APALD. The error bars indicate the standard deviation of triplicate measurements. The instinct variation on the MWCO of pristine membrane was substrate-dependent.

3.3 Correlation of pore size characteristics to permeability

391 Due to the reduced pore size and porosity in the coated membranes, their permeability
392 decreased as compared to the pristine membranes (Table 1). The coated membranes of
393 MWCO ranging from 260 to 380 Da have a permeability between 11 and 16 L m^{-2} h^{-1} bar^{-1}.

394 It was observed that the water permeability slightly decreased with incremental coating
395 cycles (Table 1). This may be because of the impregnation and deposition of precursors into
396 the porous separation layer [22, 23, 42]. A relatively long exposure time (5 s) was applied in
397 the APALD process. This promotes the diffusion of precursors into the membrane pores,
398 leading to an increased depth of deposition. A deeper impregnation and deposition of TiO_2
399 results in a greater loss of porosity in the separation layer, and therefore a lower membrane
400 permeability. Furthermore, the impregnation can occur from both the membrane surface
401 and from the support layer via intermediate layers, since the support layer of the substrate
402 was not sealed during the coating process.

403

404 Table 1. The MWCO and temperature corrected permeability of the pristine membranes, the
405 coated membranes (average ± standard deviation from at least 3 measurements).

Type of membrane	**MWCO (measured), Da**	**Permeability at 20 °C, L m^{-2} h^{-1} bar^{-1}**
450 Da CNF	490 ± 99	26 ± 7
APALD-coated CNF (1-cycle ALD coated)	287 ± 27	16 ± 5

APALD-coated CNF (2-cycle ALD coated)	333 ± 62	14 ± 0.3
APALD-coated CNF (3-cycle ALD coated)	277 ± 47	11 ± 3

406

407 The growth of the TiO_2 layer on the membrane surface may have had a negligible impact on
408 the permeability. Nikkola, et al. [44] deposited Al_2O_3 on reverse osmosis (RO) membranes
409 using 10-100 cycles of ALD. Due to the described effect of pore restriction (section 3.2), the
410 growth of Al_2O_3 occurred solely on top of the RO membrane surface. They observed that the
411 membrane permeability had minor changes when the ALD cycle number was below 50
412 (nominal coating thickness of 5 nm). When the coating cycle increased to 100, a lower
413 permeability was measured, likely due to compaction of the loosely deposited layers with
414 incremental deposition cycles. Similarly, the TiO_2 layer on the membrane surface, deposited
415 with less than or equal to 3 cycles of APALD, should have had a minor influence on the
416 permeability.

417 The commercial polymeric NF90 and NF270 nanofiltration membranes have similar MWCO,
418 200-400Da [45], to the coated tight ceramic NF membranes. However, the NF90 and NF270
419 membranes have water permeability of 7 and 12 L m^{-2} h^{-1} bar^{-1}, respectively [46], which are
420 slightly lower than the permeability of the APALD-made tight ceramic NF membranes.
421 Furthermore, the APALD-made tight ceramic NF membranes showed significantly higher
422 permeability than the sol-gel-made counterparts. Van Gestel, et al. [10] synthesized tight
423 ceramic NF membranes with a ZrO_2 separation layer via the sol-gel method; the resulting
424 membrane had a MWCO of 300 Da, but its permeability was 2.5 L m^{-2} h^{-1} bar^{-1}. The results

425 demonstrate that APALD is an effective approach for fabricating tight ceramic NF
426 membranes for water treatment. Particularly, water permeability is a crucial economic
427 factor in water treatment practices, influencing both investment and operational costs.

428 Additionally, in the water treatment systems the water permeability is strongly dependent
429 on the composition of the feed water. A significant decrease of water permeability may
430 occur when the tight ceramic NF membranes are used for filtration of real wastewater, due
431 to complex of foulants-membrane interactions (e.g. cake layer formation[17, 47-49], pore
432 blockage [50], pore narrowing due to adsorption [51, 52], calcium-bridged organic
433 fouling[47, 53-55], etc.). Further research on the performance of the tight ceramic NF
434 membranes using real (waste)water is therefore imperative.

435 An optimized, well-controlled exposure/purging sequence is crucial in the APALD procedure
436 for ceramic membranes. Kemell, et al. [28] coated Al_2O_3 to a porous material (pore size
437 approximately 2 μm), and they observed a more conforming coating inside the porous
438 material using longer purge times. Interestingly, Wang, et al. [43] suggested altering the
439 exposure time as an effective way to fine tune the growth rate in the membrane pores.
440 Further knowledge is thus required towards the optimization of exposure/purging sequence
441 times for precursors during the coating of membrane substrates using APALD, although
442 several studies have already been conducted using the conventional ALD systems operated
443 at vacuum conditions.

444

445 **4. Conclusion**

446 In this study, a new route to fabricate tight ceramic NF membranes with high water
447 permeability using atmospheric pressure atomic layer deposition (APALD) is demonstrated.

448 Utilizing APALD enables simpler and more economical processing of the membranes,
449 compared to the conventionally reported ALD schemes that typically require operation
450 under high vacuum conditions. Commercial ceramic NF membranes with an average MWCO
451 of 450 Da were coated with TiO_2. The fabricated ceramic tight NF membranes showed a
452 higher rejection of organic molecules that have molecular weights between 200 and 400 Da,
453 compared to the uncoated membranes. Their MWCO ranges from 260 to 380 Da, dependent
454 on the varied as-received substrate MWCO (400 – 600 Da).

455 The TiO_2 growth per APALD cycle is 0.39 nm on planar surfaces of silicon wafers. However, a
456 maximum one molecule of $TiCl_4$ precursor is allowed to enter the membrane pores that
457 have comparable sizes to the precursor molecular diameter. As a result, the growth rate on
458 the membrane pore walls is much lower. The average size of active pores was narrowed by
459 approximately 0.2 nm, from 0.7 nm to 0.5 nm, after one to three cycles of coating.

460 Yet, the water permeability remained high, 11 - 16 L m^{-2} h^{-1} bar^{-1}, which is higher than the
461 commercial tight polymeric NF and the sol-gel-made tight ceramic NF membranes that have
462 comparable MWCO.

463

464 **Acknowledgements**

465 This work is financed by the Dutch Technology Foundation STW (project no. 13346) and co-
466 financed by Evides Waterbedrijf N.V. and Logisticon B.V.. Ing. Marc Zuiddam and Ing.
467 Hozanna Miro at Kavli Nanolab of Delft are acknowledged for facilitating AFM and SEM
468 analyses. Dr. Jingyi Hu at Wuhan University of Technology and Dr. Rafael González Olmos at
469 IQS are acknowledged for their critical proofreading.

References

[1] H. Huang, K. Schwab, J.G. Jacangelo, Pretreatment for Low Pressure Membranes in Water Treatment: A Review, Environ. Sci. Technol., 43 (2009) 3011-3019.

[2] N. Hilal, H. Al-Zoubi, N.A. Darwish, A.W. Mohammad, M. Abu Arabi, A comprehensive review of nanofiltration membranes: Treatment, pretreatment, modelling, and atomic force microscopy, Desalination, 170 (2004) 281-308.

[3] B. Van Der Bruggen, C. Vandecasteele, T. Van Gestel, W. Doyen, R. Leysen, A review of pressure-driven membrane processes in wastewater treatment and drinking water production, Environ. Prog., 22 (2003) 46-56.

[4] J.G. Jacangelo, R. Rhodes Trussell, M. Watson, Role of membrane technology in drinking water treatment in the United States, Desalination, 113 (1997) 119-127.

[5] T. Van Gestel, C. Vandecasteele, A. Buekenhoudt, C. Dotremont, J. Luyten, B. Van der Bruggen, G. Maes, Corrosion properties of alumina and titania NF membranes, J. Membr. Sci., 214 (2003) 21-29.

[6] Y.S. Lin, I. Kumakiri, B.N. Nair, H. Alsyouri, MICROPOROUS INORGANIC MEMBRANES, Separation & Purification Reviews, 31 (2002) 229-379.

[7] P. Puhlfürß, A. Voigt, R. Weber, M. Morbé, Microporous TiO2 membranes with a cut off <500 Da, J. Membr. Sci., 174 (2000) 123-133.

[8] T. Tsuru, M. Narita, R. Shinagawa, T. Yoshioka, Nanoporous titania membranes for permeation and filtration of organic solutions, Desalination, 233 (2008) 1-9.

[9] T. Tsuru, S.-i. Wada, S. Izumi, M. Asaeda, Silica–zirconia membranes for nanofiltration, J. Membr. Sci., 149 (1998) 127-135.

[10] T. Van Gestel, H. Kruidhof, D.H.A. Blank, H.J.M. Bouwmeester, ZrO2 and TiO2 membranes for nanofiltration and pervaporation: Part 1. Preparation and characterization of a corrosion-resistant ZrO2 nanofiltration membrane with a MWCO <300, J. Membr. Sci., 284 (2006) 128-136.

[11] T. Van Gestel, C. Vandecasteele, A. Buekenhoudt, C. Dotremont, J. Luyten, R. Leysen, B. Van der Bruggen, G. Maes, Salt retention in nanofiltration with multilayer ceramic TiO2 membranes, J. Membr. Sci., 209 (2002) 379-389.

[12] T. Van Gestel, C. Vandecasteele, A. Buekenhoudt, C. Dotremont, J. Luyten, R. Leysen, B. Van der Bruggen, G. Maes, Alumina and titania multilayer membranes for nanofiltration: preparation, characterization and chemical stability, J. Membr. Sci., 207 (2002) 73-89.

[13] X. Da, J. Wen, Y. Lu, M. Qiu, Y. Fan, An aqueous sol–gel process for the fabrication of high-flux YSZ nanofiltration membranes as applied to the nanofiltration of dye wastewater, Sep. Purif. Technol., 152 (2015) 37-45.

[14] H. Qi, S. Niu, X. Jiang, N. Xu, Enhanced performance of a macroporous ceramic support for nanofiltration by using α-Al2O3 with narrow size distribution, Ceramics International, 39 (2013) 2463-2471.

[15] M. Khalili, S. Sabbaghi, M.M. Zerafat, Preparation of ceramic γ-Al2O3–TiO2 nanofiltration membranes for desalination, Chemical Papers, 69 (2015) 309-315.

[16] R. Weber, H. Chmiel, V. Mavrov, Characteristics and application of new ceramic nanofiltration membranes, Desalination, 157 (2003) 113-125.

[17] F.C. Kramer, R. Shang, S.G.J. Heijman, S.M. Scherrenberg, J.B. van Lier, L.C. Rietveld, Direct water reclamation from sewage using ceramic tight ultra- and nanofiltration, Sep. Purif. Technol., 147 (2015) 329-336.

[18] R. Shang, Ceramic ultra- and nanofiltration for municipal wastewater reuse, in, Delft University of Technology, Delft, 2014.

[19] A. Larbot, S. Alami-Younssi, M. Persin, J. Sarrazin, L. Cot, Preparation of a γ-alumina nanofiltration membrane, J. Membr. Sci., 97 (1994) 167-173.

[20] P. Marchetti, M.F. Jimenez Solomon, G. Szekely, A.G. Livingston, Molecular Separation with Organic Solvent Nanofiltration: A Critical Review, Chemical Reviews, 114 (2014) 10735-10806.

[21] S.M. George, Atomic Layer Deposition: An Overview, Chemical Reviews, 110 (2010) 111-131.

[22] F. Li, Y. Yang, Y. Fan, W. Xing, Y. Wang, Modification of ceramic membranes for pore structure tailoring: The atomic layer deposition route, J. Membr. Sci., 397–398 (2012) 17-23.
[23] Z. Song, M. Fathizadeh, Y. Huang, K.H. Chu, Y. Yoon, L. Wang, W.L. Xu, M. Yu, TiO2 nanofiltration membranes prepared by molecular layer deposition for water purification, J. Membr. Sci., 510 (2016) 72-78.
[24] H. Van Bui, F. Grillo, R. Helmer, A. Goulas, J.R. van Ommen, Controlled Growth of Palladium Nanoparticles on Graphene Nanoplatelets via Scalable Atmospheric Pressure Atomic Layer Deposition, The Journal of Physical Chemistry C, 120 (2016) 8832-8840.
[25] R. Beetstra, U. Lafont, J. Nijenhuis, E.M. Kelder, J.R. van Ommen, Atmospheric Pressure Process for Coating Particles Using Atomic Layer Deposition, Chemical Vapor Deposition, 15 (2009) 227-233.
[26] A. Goulas, R. van Ommen, Atomic layer deposition of platinum clusters on titania nanoparticles at atmospheric pressure, Journal of Materials Chemistry A, 1 (2013) 4647-4650.
[27] D. Valdesueiro, M.K. Prabhu, C. Guerra-Nunez, C.S.S. Sandeep, S. Kinge, L.D.A. Siebbeles, L.C.P.M. de Smet, G.M.H. Meesters, M.T. Kreutzer, A.J. Houtepen, J.R. van Ommen, Deposition Mechanism of Aluminum Oxide on Quantum Dot Films at Atmospheric Pressure and Room Temperature, The Journal of Physical Chemistry C, 120 (2016) 4266-4275.
[28] M. Kemell, M. Ritala, M. Leskelä, R. Groenen, S. Lindfors, Coating of Highly Porous Fiber Matrices by Atomic Layer Deposition, Chemical Vapor Deposition, 14 (2008) 347-352.
[29] J. Shirley, S. Mandale, V. Kochkodan, Influence of solute concentration and dipole moment on the retention of uncharged molecules with nanofiltration, Desalination, 344 (2014) 116-122.
[30] B. Van der Bruggen, C. Vandecasteele, Modelling of the retention of uncharged molecules with nanofiltration, Water Res, 36 (2002) 1360-1368.
[31] F.P. Cuperus, D. Bargeman, C.A. Smolders, Permporometry: the determination of the size distribution of active pores in UF membranes, J. Membr. Sci., 71 (1992) 57-67.
[32] G.Z. Cao, J. Meijernik, H.W. Brinkman, A.J. Burggraaf, Permporometry study on the size distribution of active pores in porous ceramic membranes, J. Membr. Sci., 83 (1993) 221-235.
[33] S.J. Gregg, K.S.W. Sing, Adsorption, Surface Area and Porosity. 2nd Edition, Academic Press, London, 1982.
[34] X. Liang, R.L. Patel, Porous titania microspheres with uniform wall thickness and high photoactivity, Ceramics International, 40 (2014) 3097-3103.
[35] K. Nevalainen, N. Isomäki, M. Honkanen, R. Suihkonen, T. McNally, E. Harkin-Jones, S. Syrjälä, J. Vuorinen, P. Järvelä, Melt-compounded nanocomposites of titanium dioxide atomic-layer-deposition-coated polyamide and polystyrene powders, Polymers for Advanced Technologies, 23 (2012) 357-366.
[36] Y. Lei, B. Liu, J. Lu, R.J. Lobo-Lapidus, T. Wu, H. Feng, X. Xia, A.U. Mane, J.A. Libera, J.P. Greeley, J.T. Miller, J.W. Elam, Synthesis of Pt–Pd Core–Shell Nanostructures by Atomic Layer Deposition: Application in Propane Oxidative Dehydrogenation to Propylene, Chem. Mater., 24 (2012) 3525-3533.
[37] X. Sun, M. Xie, G. Wang, H. Sun, A.S. Cavanagh, J.J. Travis, S.M. George, J. Lian, Atomic Layer Deposition of TiO2 on Graphene for Supercapacitors, J. Electrochem. Soc., 159 (2012) A364-A369.
[38] Y. Lei, J. Lu, H. Zhao, B. Liu, K.-B. Low, T. Wu, J.A. Libera, J.P. Greeley, P.J. Chupas, J.T. Miller, J.W. Elam, Resolving Precursor Deligation, Surface Species Evolution, and Nanoparticle Nucleation during Palladium Atomic Layer Deposition, J. Phys. Chem. C, 117 (2013) 11141-11148.
[39] C. Ban, M. Xie, X. Sun, J.J. Travis, G. Wang, H. Sun, A.C. Dillon, J. Lian, S.M. George, Atomic layer deposition of amorphous TiO_2 on graphene as an anode for Li-ion batteries, Nanotechnology, 24 (2013) 424002.
[40] R.B. King, J.K. Burdett, R.H. Crabtree, C.M. Lukehart, R.A. Scott, R.L. Wells, Encyclopedia of Inorganic Chemistry, Wiley, 1998.
[41] M.A. Cameron, I.P. Gartland, J.A. Smith, S.F. Diaz, S.M. George, Atomic Layer Deposition of SiO2 and TiO2 in Alumina Tubular Membranes: Pore Reduction and Effect of Surface Species on Gas Transport, Langmuir, 16 (2000) 7435-7444.
[42] F. Li, L. Li, X. Liao, Y. Wang, Precise pore size tuning and surface modifications of polymeric membranes using the atomic layer deposition technique, J. Membr. Sci., 385–386 (2011) 1-9.

572 [43] Q. Wang, X. Wang, Z. Wang, J. Huang, Y. Wang, PVDF membranes with simultaneously enhanced
573 permeability and selectivity by breaking the tradeoff effect via atomic layer deposition of TiO2, J.
574 Membr. Sci., 442 (2013) 57-64.
575 [44] J. Nikkola, J. Sievänen, M. Raulio, J. Wei, J. Vuorinen, C.Y. Tang, Surface modification of thin film
576 composite polyamide membrane using atomic layer deposition method, J. Membr. Sci., 450 (2014)
577 174-180.
578 [45] Dow, What is the MWCO of FILMTECTM NF90 and NF270 Reverse Osmosis Elements?, in, 2015.
579 [46] A. Simon, J.A. McDonald, S.J. Khan, W.E. Price, L.D. Nghiem, Effects of caustic cleaning on pore
580 size of nanofiltration membranes and their rejection of trace organic chemicals, J. Membr. Sci., 447
581 (2013) 153-162.
582 [47] A.I. Schäfer, U. Schwicker, M.M. Fischer, A.G. Fane, T.D. Waite, Microfiltration of colloids and
583 natural organic matter, J. Membr. Sci., 171 (2000) 151-172.
584 [48] G. Amy, Fundamental understanding of organic matter fouling of membranes, Desalination, 231
585 (2008) 44-51.
586 [49] M.D. Kennedy, J. Kamanyi, B.G.J. Heijman, G. Amy, Colloidal organic matter fouling of UF
587 membranes: role of NOM composition & size, Desalination, 220 (2008) 200-213.
588 [50] H. Huang, T.A. Young, J.G. Jacangelo, Unified membrane fouling index for low pressure
589 membrane filtration of natural waters: Principles and methodology, Environmental Science and
590 Technology, 42 (2008) 714-720.
591 [51] R. Shang, F. Vuong, J. Hu, S. Li, A.J.B. Kemperman, K. Nijmeijer, E.R. Cornelissen, S.G.J. Heijman,
592 L.C. Rietveld, Hydraulically irreversible fouling on ceramic MF/UF membranes: Comparison of fouling
593 indices, foulant composition and irreversible pore narrowing, Sep. Purif. Technol., 147 (2015) 303-
594 310.
595 [52] C. Jucker, M.M. Clark, Adsorption of aquatic humic substances on hydrophobic ultrafiltration
596 membranes, J. Membr. Sci., 97 (1994) 37-52.
597 [53] S. Li, S.G.J. Heijman, J.Q.J.C. Verberk, P. Le Clech, J. Lu, A.J.B. Kemperman, G.L. Amy, J.C. van Dijk,
598 Fouling control mechanisms of demineralized water backwash: Reduction of charge screening and
599 calcium bridging effects, Water Res, 45 (2011) 6289-6300.
600 [54] L. Fan, J.L. Harris, F.A. Roddick, N.A. Booker, Influence of the characteristics of natural organic
601 matter on the fouling of microfiltration membranes, Water Res, 35 (2001) 4455-4463.
602 [55] Y. Wang, C. Combe, M.M. Clark, The effects of pH and calcium on the diffusion coefficient of
603 humic acid, J. Membr. Sci., 183 (2001) 49-60.

604

605